

1
2
3
4 **Digital Imaging Mass Spectrometry**
5
6
7

8
9
10 Running title: Digital Imaging Mass Spectrometry
11

12
13
14 Casimir Bamberger¹, Uwe Renz², and Andreas Bamberger²
15
16
17

18
19 ¹ Department of Chemical Physiology, The Scripps Research Institute, 10550
20 North Torrey Pines, La Jolla, CA 92037, USA.
21

22
23 ² Physics Institute, Albert-Ludwigs University of Freiburg, Hermann-Herder-
24 Strasse 3a, 79104 Freiburg, Germany.
25
26
27
28
29
30
31

32 ***Address reprint requests to:***
33

34
35 Dr. Casimir Bamberger
36

37 Department of Chemical Physiology, The Scripps Research Institutes,
38 10550 North Torrey Pines, La Jolla, CA 92037, USA
39

40
41 Phone: +1-858-784-7645
42

43
44 Fax: +1-858-784-8883
45

46
47 cbamberg@scripps.edu
48
49
50
51
52

53 ***Key words:*** ASIC, Timepix, biomolecules, digital array detector
54
55
56
57
58
59
60
61
62
63
64
65

Abstract

Methods to visualize the two-dimensional distribution of molecules by mass spectrometric imaging evolve rapidly and yield novel applications in biology, medicine, and material surface sciences. Most mass spectrometric imagers acquire high mass resolution spectra spot-by-spot and thereby scan the object's surface. Thus, imaging is slow and image reconstruction remains cumbersome. Here we describe an imaging mass spectrometer that exploits the true imaging capabilities by ion optical means for the time of flight mass separation. The mass spectrometer is equipped with the ASIC Timepix chip as an array detector to acquire the position, mass, and intensity of ions that are imaged by MALDI directly from the target sample onto the detector. This imaging mass spectrometer has a spatial resolving power at the specimen of (84 ± 35) μm with a mass resolution of 45 and locates atoms or organic compounds on a surface area up to ~ 2 cm^2 . Extended laser spots of ~ 5 mm^2 on structured specimens allowed parallel imaging of selected masses. The digital imaging mass spectrometer proves high hit-multiplicity, straightforward image reconstruction and its potential for high-speed readout at 4 kHz or more. This device demonstrates a simple way of true image acquisition like a digital photographic camera. The technology may enable a fast analysis of biomolecular samples in near future.

Introduction

Imaging mass spectrometry is a widely used tool for detecting the molecular composition of sample surfaces [1-6] with a two-dimensional resolution in the μm range [7]. The technology has been proven valuable for many fields of application, ranging from diagnostics in microchip production to analysis of tissue samples. Mass spectrometric images visualize the spatial distribution of molecules with a set of four parameters: two for the spatial dimensions, one for molecules' molecular mass, and one for its abundance.

The commonly used imaging methodology is scanning or micro probing, which first records mass and intensity of molecules or atoms spot-by-spot, and then reconstructs their two-dimensional distribution in a mass spectrometric image [8]. Here, an alternative approach is presented: The two-dimensional distribution of molecules or atoms is acquired in the first step, and their abundance is accumulated by subsequent measurement cycles. The advantage is the parallel acquisition of mass spectrometric data from an extended sample surface [9]. A separation of masses with the time of flight (TOF) principle favors this purpose, since the spatial information can be mapped onto the detector through ion optics. For example, this approach is realized in mass spectrometers of the TRIFT series (Physical Electronics) in the stigmatic mode: Blankers in the ion path set a narrow m/z -range and the spatial distribution of ions is derived from a read out of a phosphor screen by a CCD camera [10, 11]. Alternatively, delay-line read out may be utilized to record the time of flight of spatially separated ions in a single measurement cycle [12]. However, array detectors of high multiplicity offer an attractive and straight-forward realization.

Indeed, the recent development of a time sensitive, highly pixilated detector (Timepix), which was first conceived for 3D-reconstruction of particle tracks [13, 14] and is meanwhile used for photon detection [15, 16], provides a perfect solution. Herein we describe, for the first time to our knowledge, the application of the Timepix detector for imaging mass spectrometry. Recently, the precursor to the Timepix, the Medipix was tested for its application to mass spectrometric imaging, although lacking temporal resolving capabilities [17]. The Timepix detector covers a sensitive surface of $14 \times 14 \text{ mm}^2$ with a matrix of 256×256 pixels. Each pixel occupies $55 \times 55 \mu\text{m}^2$ and detects either charge through time over threshold (TOT) or the time of arrival (TIME) of a signal.

For a proof of principle a linear time of flight mass spectrometer was assembled. Its basic elements were a MALDI driven ion source, a drift space with a focusing ion optics, a multi channel plate (MCP), and the Timepix. The electron signal generated by ions at the MCP covers several pixels of the Timepix, which allows for neighboring pixels to record TOT and TIME in an alternating fashion. As a benefit the simultaneous recording of the electron signal with several pixels allows the reconstruction of the time of arrival with higher precision [18].

The following set of experiments shows the feasibility of this digital mass imaging approach. The mass resolution and imaging properties of the Timepix are presented and the results are discussed within the scope of possible improvements for biological and biomedical applications.

Material and Methods

The Time of Flight Mass Spectrometer and one Event Cycle

The imaging mass spectrometer apparatus comprises a N₂ laser with optics, sample plate with MALDI analyte, drift volume, and detection system as depicted in Figure 1a and described in supplemental materials and methods. The recipient, the acceleration stage (73 mm), the drift space (117 mm) and the MCP, which is part of the detection system, have been retrieved and modified from an experimental setup used previously to analyze the dynamics of molecular interactions [19].

The laser pulse set the reference time and triggered the shutter gate for the Timepix chip (see supplemental material and methods for detailed description of the Timepix). The logic for each pixel provided optionally two modes of operation TIME and TOT (Figure 1b). A shutter gate of fixed length (~10 μ s) was applied at the time the laser had fired accepting a charge signal above threshold. From this moment on the 13.5 bit register stored the number of clock cycles (clock speed between 70 and 80 MHz) until either the end of the shutter gate was reached (TIME) or the charge signal dropped below threshold (TOT).

In the final experiment with the extended laser area the grid terminating the drift space was removed to avoid possible interference of micro-lensing with experiments using a highly structured target, thereby slightly modifying the ion optics (Supplemental materials and methods, and supplemental Figure 1).

Data Analysis

The events were processed with MATLAB 7 (The Mathworks) separating the two modes TIME and TOT and searching for contiguous areas of hits originating from ion signals, subsequently called clusters (see also supplemental materials and methods). The intensity of the ion signal was determined from the sum of the TOT counts in the cluster and the spatial position from the centre of gravity. All clusters, above a predetermined cluster size, were stored along with its spatial position, signal intensity, and time of arrival data for further analysis.

Results

In order to show the applicability of the Timepix detector for biomolecular imaging mass spectrometry, the imaging mass spectrometer was equipped with focusing ion optics for imaging purposes. An initial set of mass spectra was acquired without activation of the Einzel lens, i.e. in a non-focusing mode and without the diaphragm. MALDI-matrix embedded Cesium ($m/z \sim 133$) or Caffeine ($m/z \sim 194$), or a mixture of both was deposited on the target sample plate. Depending on the energy of the UV-laser pulse, multiple Caffeine or Cesium ions were extracted simultaneously by MALDI from the target sample in one event.

Cluster Shapes and Multiplicity

As expected for MALDI ionization, the number of ions detected varied depending on laser intensity and location on the target sample plate. Events recording up to 200 ions resulted in mostly well-separated clusters generated from individual ions as shown in Figure 2a. It demonstrates the capability of the device to record events with high ion multiplicity, which is limited only by excessive overlap of

1
2
3
4 clusters. The separation of clusters depends on the cluster size and the multiplicity (see
5
6 supplemental results). Small cluster sizes are preferred in order to achieve high
7
8 multiplicities resulting from increased laser intensities. Because the events shown are
9
10 recorded in non-focusing mode of the mass spectrometer, the spatial distribution of
11
12 clusters reflects the dispersion of ions caused by the initial transverse momentum
13
14 obtained during the MALDI ionization process.
15
16
17

18
19 For each recorded event the number of observed clusters was determined. Here
20
21 more than five adjacent, recording pixels were required for a cluster. Figure 2b depicts
22
23 a close-up of the matrix TIME for several clusters recorded. The clusters in the TIME
24
25 matrix have column-like shape with a flat plateau extending over several pixels due to
26
27 the simultaneous arrival time of the electrons. The corresponding clusters in the TOT
28
29 matrix are shaped in Gaussian profiles reflecting the two-dimensional projection of the
30
31 cloud of electrons leaving the MPC (Figure 2c). The event of Figure 2a is displayed in
32
33 a three-dimensional representation in Figure 2d, which visualizes that the Caffeine
34
35 signal is well separated from background.
36
37
38
39
40

41 ***Acquisition of Mass Spectra***

42
43
44 The m/z value for each detected ion was calculated from the corrected TIME
45
46 signal (“time walk” correction, see supplemental results and supplemental Figure 3a)
47
48 and all m/z values were plotted in a histogram to obtain the final mass spectrum for a
49
50 series of events recorded (Figure 3a). In this example, two significant peaks appear,
51
52 which correspond to single-charged Caffeine ($m/z \sim 195$) and Iron ($m/z \sim 56$), which
53
54 represents an ionization by-product from the stainless steel backing of the sample.
55
56
57
58
59
60
61
62
63
64
65

1
2
3
4 In a TOF mass spectrometer, the resolution and the accuracy of mass
5
6 determination are dependent on (1) the dimensions of the mass analyzer and (2) the
7
8 precision of the time to digital converter. In order to assess the influence of these
9
10 parameters for the small time of flight mass spectrometer presented, the shape and
11
12 position of the Caffeine peak was determined by fitting a Gaussian to the data points
13
14 (Figure 3b). The average time of flight for Caffeine was $9.610 \pm 0.138 \mu\text{s}$ and a signal
15
16 dispersion of $\Gamma = 115 \text{ ns}$. Based on the full width at half maximum (FWHM) for
17
18 Caffeine, a mass resolution of $45 \text{ m}/\Delta\text{m}$ was determined at m/z 195 (Figure 3b). It
19
20 should be mentioned that the resolution was not limited by the clock speed (see
21
22 supplemental results) and no delayed extraction has been applied which is well known
23
24 to increase mass precision. The overall calibration of the mass spectrometer is
25
26 demonstrated using three different ions, namely Iron, Cesium and Caffeine
27
28 (supplemental Figure 3b).
29
30
31
32
33
34
35
36

37 ***Spatial Resolution of the Detector System***

38
39 As shown in Figure 1a the field-free section for the ion drift is terminated by a
40
41 grounded grid, followed by the post acceleration stage of -2.5 kV . As a result of the
42
43 field gradient, micro-lensing occurred at the detector plane causing the Cesium ion
44
45 intensities to peak in a periodic pattern when observed over a large number of events
46
47 (Figure 3c). Using this image of the grid structure, it was possible to estimate the
48
49 spatial resolution of the combined MCP-Timepix detector system. The analysis of the
50
51 Cs^+ ion intensity pattern with properly chosen angle of projection revealed periodic
52
53 intensity maxima with a step size of 0.22 mm , which closely matched the periodicity
54
55 of the grid. Based on the lateral discrimination capability determined from the Cesium
56
57
58
59
60
61
62
63
64
65

intensity pattern, the detector provides an estimated spatial resolution of $\sigma = 36 \mu\text{m}$. Indeed, the spatial resolution is smaller than the lateral extension of a single detector pixel ($55 \mu\text{m}$), which is due to the fact that the center of gravity is determined with cluster sizes being spread over several pixels.

The imaging capability of the detector section only was visualized in an additional experiment: A copper-coated PC board with 0.2 mm pinholes separated by $\geq 0.6 \text{ mm}$ depicting the letters of the word “IMAGE” was positioned near the grid at the end of the drift tube. The passage of mass selected Cs ions through the pinholes reveals the word IMAGE on the detector plane with 10^3 events (Figure 3d).

This first set of experiments showed that a mass spectrometric detector based on the Timepix is capable of spatially resolving a distribution of ions while determining m/z values at the same time. The analysis of individual clusters recorded in large numbers with each event allowed a fast data acquisition and collection of mass spectra. The simultaneous measurement of TIME and TOT can improve the precision in the m/z -measurement introduced by the finite rise time of the input circuit.

Imaging of Laser Spots on the Target Surface

The instrument provided also a two-dimensional resolution at the target side, which is a prerequisite for imaging. As mentioned above an Einzel lens mapped the ion-optical image of the target plate onto the detector surface. A SIMION 7 simulation verified that the ion optical image was de-magnified by a factor of 2.2 as a consequence of the acceleration stage and the Einzel lens being positioned near the front end of the drift volume. A diaphragm ($\varnothing 6 \text{ mm}$) was introduced near the

1
2
3
4 entrance grid of the drift tube to keep astigmatic distortions small. Following
5
6 activation of the Einzel lens, Caffeine-ions generated with a laser spot of small size
7
8 were focused by the ion optical system onto the detector system in a point like spot
9
10 (supplemental Figures 4a, b).
11
12

13
14 To show the imaging capabilities of the mass spectrometer Cs^+ ions were
15
16 generated by MALDI at two distinct positions on the target plate by displacing the
17
18 laser spot. First, the optical focusing of the laser was checked for its quality by
19
20 estimating its visual transverse extension at the target plate. It was found to be less
21
22 than $0.3 \times 0.3 \text{ mm}^2$. After recording the mass spectrum at the first position, the laser
23
24 spot was moved by displacing the lens vertically along the y-axis of the target plate by
25
26 $\sim 1.0 \text{ mm}$. Due to geometric constraints for the mounting of the Timepix chip its axes
27
28 are rotated by 135° relative to the target reference system. Therefore, the imaged spot
29
30 was displaced in both axes of the Timepix reference frame, – by 0.3 mm along the x-
31
32 axis (Figure 4a) and 0.2 mm along the y-axis (Figure 4b). The resulting ion optical
33
34 image for Cs^+ -ions was shifted diagonally by about 0.37 mm on the Timepix detector
35
36 with an average standard deviation of the Gaussian fits for both spots of $38.1 \mu\text{m}$.
37
38 Concluding from the distinct positions of two spots the imaging mass spectrometer
39
40 can resolve two spatially separated positions at the sample surface.
41
42
43
44
45
46
47

48 Subsequently we determined the spatial resolution and its error with respect to
49
50 the sample plate. To this end, a more refined estimation of the average standard
51
52 deviation was performed taking into account, that micro-lensing occurs at the detector
53
54 stage as described above. By considering the maximum contribution of micro-lensing
55
56 to the change of the spot width, the resolution with a systematic error was determined
57
58
59
60
61
62
63
64
65

1
2
3
4 to (38.1 ± 16.0) μm . Due to the demagnification of the system the resolution at the
5
6 sample plate achieved in this experiment is (84 ± 35) μm . A possible contribution due
7
8 to the MPCs' finite channel diameter of <10 μm is neglected. Whereas a spatial
9
10 resolution of the digital imaging mass spectrometer is demonstrated in this
11
12 experiment, the precision of the spatial resolution might be affected by additional
13
14 factors such as the extension and spatial intensity variations of the laser spot on the
15
16 target sample plate.
17
18
19
20
21

22 ***Imaging of a Two-dimensional Structure on the Target by*** 23 24 ***Extended Illumination***

25
26
27 The following set of experiments addresses the simultaneous imaging of an
28
29 extended target plate area in macroscopic scale. For an illumination of an extended
30
31 surface, the Nitromite N_2 -laser was replaced by a high power N_2 -laser providing
32
33 effective beam energy up to 2 mJ. This allowed for an increase of the illuminated area
34
35 to an approximate rectangle of $\sim(5 \times 2)$ mm^2 (see supplemental Figure 5b).
36
37
38

39
40 The first experiment assessed the general imaging capability of the mass
41
42 spectrometer with the grid at the end of the drift volume in place. The target consisted
43
44 of Cesium embedded in a MALDI matrix deposited on a circular plateau of 3 mm \varnothing ,
45
46 which is separated from the remainder of the flat target plate by a circular groove of
47
48 1 mm width (Figure 5a, inset). During target preparation the matrix crystallized
49
50 preferentially close to the rims of the groove. Imaging of the macroscopic structure on
51
52 the target plate was achieved along the major axis of the defocused UV-laser beam
53
54 directly, and along the minor axis by step-wise displacement of the beam between
55
56 each measurement cycle while the number of measured events was kept equal and the
57
58
59
60
61
62
63
64
65

1
2
3
4 ion optics unaltered. All data acquired was merged to one dataset, which finally
5
6 reproduced the original ring-like deposition of Cs on the sample plate for the Cs⁺ line
7
8 in the mass spectrum (Figure 5a). The same experimental procedure revealed an even
9
10 distribution of Iron background from an ion image taken from the untreated flat
11
12 stainless steel plate (supplemental Figure 5a). The spatial frequency distribution of Cs⁺
13
14 signals correlates with the density of Cs⁺/MALDI-matrix as observed by a light image
15
16 of the target plate surface. Note that the signal of Cs⁺ shows a rarified intensity in the
17
18 center of the disk similar to the Cesium deposit seen in the photograph of the target.
19
20
21 The correlation observed between the initial deposition of Cesium and the mass
22
23 spectrometric image indicates that the digital imaging mass spectrometer can be used
24
25 to collect information about the spatial distribution of molecules or atoms in a
26
27 quantitative manner.
28
29
30
31
32

33 In a second experiment, the spatial resolution was tested by imaging isolated spots of
34
35 analyte deposited onto a stainless steel plate. The setup was modified so micro-lensing
36
37 was suppressed (See supplemental material and methods, and supplemental
38
39 Figure 1b). A MALDI target with a regular spacing of spots was produced by ink jet
40
41 printing [20] of Cesium-containing MALDI matrix onto the stainless steel target plate.
42
43 Dots were deposited in a rectangular grid with a pitch of 1.6 mm onto the Fe backing
44
45 (Figure 5b, inset). Figure 5b shows the spatial distribution of the Cesium-MALDI-
46
47 matrix initially deposited by the printer (white spots). The nominal regular structure of
48
49 Cesium depositions (yellow disks) and the spatial distribution of Cesium signal
50
51 recorded by the Timepix detector (red dots) is superimposed on the photograph of the
52
53 sample plate. The laser image was displaced on the target once by ~0.5 mm during
54
55
56
57
58
59
60
61
62
63
64
65

1
2
3
4 image acquisition and the Iron background signal for one of the two laser positions is
5
6 shown in supplemental Figure 5b. Regions of high Cesium content closely match the
7
8 original depositions of the Cesium-MALDI-matrix mixture.
9

10
11 Both sets of experiments show the feasibility to image two-dimensional
12
13 samples with an extended laser spot and the mass spectrometric images reproduce the
14
15 initial spatial distributions of the analyte on the target sample plate. The beam energy
16
17 per pulse limited the sampled surface to about 5-10 mm². Therefore, we employed the
18
19 scanning method in order to cover still larger surfaces, but ionization sources with
20
21 higher energy fluxes are readily available from other laser sources e.g. tripled
22
23 NdYAG-lasers.
24
25
26
27

28 **Discussion and Conclusion**

29
30 In summary, the Timepix chip was successfully operated as an array detector
31
32 in a small linear TOF mass spectrometer. The mass spectrometer imaged the spatial
33
34 distribution of atoms and small organic molecules with sufficiently high mass
35
36 resolution. It demonstrated that the acquisition of mass spectrometric images is
37
38 possible with ion detection using front-end digitization and highly pixilated sensors.
39
40 The Timepix offers the capability of high event rates up to 4 kHz [21] and allows very
41
42 fast data acquisition with an appropriate interface for data transfer. The experimental
43
44 setup presented here was not optimized for fast data acquisition, since more advanced
45
46 USB-based readout modules are currently being developed [22].
47
48
49
50
51

52
53 The scanning method and delay line readout approach realized in conventional
54
55 mass spectrometric imaging obtains positional information indirectly. In contrast,
56
57 highly pixilated detectors directly record all four parameters necessary to acquire mass
58
59
60
61

1
2
3
4 spectrometric images (position, m/z value, and intensity) thereby omitting
5
6 cumbersome reconstruction means. Key advantages are (1) multi-hit capability up to
7
8 200 ions per event with (2) a lateral resolution of 36 μm of the detector stage. We
9
10 achieved a lateral resolution of 84 μm at the target sample plate, which is mainly
11
12 constrained by the de-magnifying ion optical system presently used. It should be
13
14 stressed that the ion optical demagnification in this setup is unfavorable for
15
16 demonstrating a high resolution power on the sample due to both the extended
17
18 acceleration stage and as well as the small drift distance. There are ion optical
19
20 focusing systems with multiple lenses available [23], which would provide higher
21
22 magnifications thereby increasing the spatial resolution at the target.
23
24
25
26
27

28
29 Timepix chips can be seamlessly attached at three sides to expand the detector
30
31 surface (e.g. quadruplets or higher) thereby increasing either the overall multi-hit
32
33 capability of the system or the spatial resolution at the target depending on the setting
34
35 of the ion optics. Although the multi-hit capability of a pixel detector clearly offers the
36
37 advantage of parallel ion detection, it seems to be limited by the need of a finite cluster
38
39 size in the mixed mode operation to reconstruct an accurate m/z value and position of
40
41 the ion signal. However, data acquisition in purely TIME sensitive mode offers a
42
43 spatial reconstruction marginally worse than with a mixed mode operation. In order to
44
45 get a time walk correction, the number of pixels in TOT-mode may be reduced in
46
47 favor of an increased time precision. Moreover, variations in cluster size at small MPC
48
49 signals are not negligible and more sophisticated algorithms for the separation of
50
51 partially overlapping clusters are developed.
52
53
54
55
56
57
58
59
60
61
62
63
64
65

1
2
3
4 We estimated the speed and limits of data taking based on the multiplicities of
5
6 registered ions, which might well be in the region of several hundred per laser shot as
7
8 shown. If only one dominant ion species would be analyzed, the data rate increases
9
10 approximately 200 fold per laser shot, provided space-like overlap of ion-induced
11
12 clusters would be acceptable. Taking into account a maximum laser repetition rate of
13
14 ~ 4 kHz, the total improvement in data acquisition speed would be a factor 1000 when
15
16 compared with conventional micro probing. For the Timepix the data volume is
17
18 2 Gb/s, which can be handled easily for transfer and storage. The data volume to be
19
20 processed is sizable, since the parameters of all clusters per readout cycle have to be
21
22 determined. Typically such a task can be handled by computing farms using optimized
23
24 algorithms.
25
26
27
28
29
30

31 In fact, the data volume would be higher when allowing also the detection of
32
33 ions with different arrival times impinging at the same position of the detector.
34
35 However, the Timepix is designed in principle with a single hit feature. Of course a
36
37 Timepix with multi-hit capability for all pixels would eventually avoid the application
38
39 of narrow mass windows (see also supplemental discussion).
40
41
42

43 Modern MALDI scanning mass spectrometric imagers achieve a spatial
44
45 resolution of typically ~ 150 μm [24] at the sample-stage dictated by the step size.
46
47 Using a differential scanning method a resolution of less than 10 μm has been
48
49 demonstrated [7]. With appropriate sample ionization, the digital imaging mass
50
51 spectrometer presented here can achieve comparable spatial resolution. The spatial
52
53 resolution at the sample depends on the ion optics of the imaging TOF mass
54
55 spectrometer. Indeed, time of flight mass spectrometers with a magnification up to 300
56
57
58
59
60
61
62
63
64
65

1
2
3
4 are realized in commercially available instruments of the TRIFT-series. The
5
6 combination of appropriate ion optics with the highly parallel detection principle will
7
8 promote digital imaging mass spectrometry as high throughput instrumentation in the
9
10 future.
11

12
13
14 The digital imaging TOF as presented here is limited in spectral resolution
15
16 ($m/\Delta m$ 45 at 195 m/z). There are two essential reasons: the short drift path (0.12 m)
17
18 and the lack of velocity focusing. The digital imaging mass spectrometer was not
19
20 equipped to correct for initial differences in kinetic energy with the delayed extraction
21
22 principle, which in general improves spectral resolution. In addition, the time to digital
23
24 converter (TDC) in the Timepix is restricted to ~ 100 MHz, a factor 100 lower than the
25
26 time resolution of modern TDCs used in non-imaging TOF mass spectrometers.
27
28 Therefore, spatial resolution rather than spectral resolution using the Timepix opens an
29
30 interesting field of mass spectrometric applications.
31
32

33
34
35 The MALDI process was adopted to generate ions on an extended surface
36
37 because MALDI efficiently ionizes biomolecules and is well employed together with
38
39 the time of flight mass spectrometry for imaging applications [25]. It is not excluded
40
41 that the MALDI process has some intrinsic limit for the spatial resolution [26] as well
42
43 as a transformation of the analyte by crystallization seems to be necessary. With
44
45 respect to imaging applications, the efficiency and reproducibility of the sample
46
47 ionization is dependent on many variables introduced during sample preparation and
48
49 ionization (see supplemental discussion). Another field of application is SIMS using
50
51 fullerenes, where an improvement of spatial resolution with ion optical imaging and
52
53 digital readout with the Timepix is expected.
54
55
56
57
58
59
60
61
62
63
64
65

1
2
3
4 In conclusion, the digital mass spectrometer presented here proved the
5
6 principle of highly parallel mass spectrometric image acquisition. Thereby it opens the
7
8 door for high throughput sample analysis by imaging ions extracted from extended
9
10 sample surfaces. Based on the achieved spatial ion multiplicity and the potential
11
12 readout rates the true mass spectrometric imaging principle presented here allows an
13
14 increase of data taking speed of several orders of magnitude over micro probing.
15
16 Moreover, the technology may enable a fast analysis of samples spotted in arrays,
17
18 eventually illuminated with a bundle of laser beams. Although with limited spectral
19
20 resolution, the digital imaging mass spectrometer may have broad range of
21
22 applications ranging from biological and medical experimentation, material sciences
23
24 to forensic analysis.
25
26
27
28
29
30
31
32

33 **Acknowledgements**

34
35
36 The provision of Timepix chips through the MEDIPIX-collaboration/EUDET-
37
38 collaboration and its expertise is greatly appreciated. Many thanks for Andreas
39
40 Zwerger being helpful for Timepix related chip mounting and software
41
42 implementation. The workshops of the Physics Institute, University of Freiburg have
43
44 provided a perfect support. Prof. Bernd v. Issendorff was helpful providing advices
45
46 and ion optical simulation programs. We are grateful to Prof. Rüdiger Brenn for
47
48 providing main parts of time of flight spectrometer. The help of Dr. Sandra Pankow
49
50 throughout all steps of the project is greatly appreciated.
51
52

53
54
55 Idea and experimental design were developed by A.B. and C.B., software
56
57 development and noise-free calibration of pixels was performed by U.R., instrument
58
59
60
61
62
63
64
65

1
2
3
4 setup and data taking were performed by A.B. and C.B., manuscript was prepared by
5
6
7 A.B. and C.B.

8 9 **Legends for Figures**

10 11 **Figure 1**

12
13
14
15 **Schematic of a time-of-flight mass spectrometer with high multiplicity**
16
17
18 **detector array and representation of one measurement cycle. (a)** The major
19
20 components of the time-of-flight mass spectrometer are the acceleration stage
21
22 (horizontal black, thick, long-dashed lines), the drift volume with the Einzel lens
23
24 (horizontal black, thin, long-dashed lines), the drift volume with the Einzel lens
25
26 between the grids (vertical dotted lines) and the detector section. The black dashed line
27
28 indicates the path of ions generated off-axis and focused on the Timepix chip. The N₂-
29
30 laser beam (grey arrow) releases ions by MALDI on the sample plate with a focused
31
32 spot or with an extended area by adjusting the laser optics (Einzel lens). **(b)** The time
33
34 sequence starts with opening the shutter gate triggered by the laser pulse (vertical
35
36 arrowhead). TOT determines approximately the charge of the signal and TIME serves
37
38 to determine the time of flight after correcting for the gate length. The black dashed
39
40 line indicates the minimal charge necessary to trigger detection whereas black bars
41
42 represent the opening time of the shutter, the stored number of cycles (TIME or TOT)
43
44 and deduced time of flight (TOF). Numbers given to the right exemplify the measured
45
46 value based on the clock cycle schematic visualized at the bottom of the graph.
47
48
49
50
51
52

53 54 **Figure 2**

55
56 **Recordings by the Timepix visualize MALDI events. (a)** The two-
57
58 dimensional representation of the detector surface shows the TOF matrix (TIME
59
60
61
62
63
64
65

converted to time of arrival) for one event of high multiplicity recorded from a Caffeine sample with the Einzel lens switched off. Clusters of pixels are visualized on the detector surface according to a rainbow-colored time code. Red clusters represent Caffeine and light blue clusters indicate Iron. **(b)** Close up of a selected x-y surface of the detector for a single laser shot. The time stamp (TIME) visualizes plateau-like shaped clusters in units of clock cycles. **(c)** The charge distribution (TOT) of the same close up shows Gaussian shaped clusters. **(d)** Three-dimensional representation of 129 individually reconstructed clusters based on (a) in terms of time walk corrected, color-coded clock cycles.

Figure 3

Digital imaging mass spectra, mass and spatial resolution, and image generating capability of the Timepix. (a) The mass spectrum (10^3 events) shows two peaks (Caffeine and Iron) above background noise. Solid red curves represent Gaussian fits. **(b)** A Gaussian curve was fitted to the frequency histogram of the drift times measured for Caffeine. The mass resolution measured was $m/\Delta m = 45$ at $m/z \sim 195$ (Caffeine+ H^+). **(c)** The frequency histogram for the Cesium ion signal visualizes the effect of micro-lensing caused by the grid at the end of the drift volume. The y-coordinate was rotated with respect to the Timepix to match the grid orientation. The peaks are fitted by multiple Gaussians (solid lines) having a resolution of $36 \mu\text{m}$. **(d)** The (x,y)-plot displays the lateral distribution of Cesium ions that were acquired with a pinhole mask depicting the word "IMAGE". The mask was positioned at the end of the drift volume.

Figure 4

Two distant spots on the target sample plate are imaged to distinct positions onto the Timepix. Frequency histograms of Cesium ions show the displacement along the x-axis **(a)** and along the y-axis **(b)** of the Timepix reference coordinate system as the laser focus was shifted by 1.0 mm at the target. Gaussian fits represent the signal intensity (rate of events) before (red) and after (violet) displacement (arrow) of the laser focus.

Figure 5

Mass spectrometric images of a ring-shaped Cesium deposition and single spots containing Cesium were acquired with an extended laser spot. (a) The mass spectrometric image visualizes the distribution of Cesium deposits on the target plate (inset). The dotted black lines indicate the projection of the target surface area onto the mass spectrometric image. Each color shows one of the 8 consecutive measurements. Between each measurement, the laser spot was shifted vertically with respect to the target plate reference system. **(b)** A Cesium-containing MALDI sample was spotted by an inkjet printer in a regular pattern (white spots) onto a stainless steel sample plate as shown in the photograph (inset). A scaled photographic image of this sample plate was overlaid with (1) the nominal position of sample spots on the sample plate (yellow) and (2) the respective mass spectrometric image of Cesium ions (red) which were acquired from two adjacent positions consecutively illuminated with the laser beam.

Literature

1. Goodwin, R. J. A.; Pennington, S. R.; Pitt, A. R., Protein and peptides in pictures: Imaging with MALDI mass spectrometry. *Proteomics* **2008**, *8* (18), 3785-3800.
2. Walch, A.; Rauser, S.; Deininger, S. O.; Hofler, H., MALDI imaging mass spectrometry for direct tissue analysis: a new frontier for molecular histology. *Histochem Cell Biol* **2008**, *130* (3), 421-434.
3. Hardesty, W. M.; Caprioli, R. M., In situ molecular imaging of proteins in tissues using mass spectrometry. *Anal Bioanal Chem* **2008**, *391* (3), 899-903.
4. Cornett, D. S.; Reyzer, M. L.; Chaurand, P.; Caprioli, R. M., MALDI imaging mass spectrometry: molecular snapshots of biochemical systems. *Nat Methods* **2007**, *4* (10), 828-833.
5. Cooks, R. G.; Ouyang, Z.; Takats, Z.; Wiseman, J. M., Detection Technologies. Ambient mass spectrometry. *Science* **2006**, *311* (5767), 1566-1570.
6. Roggli, V. L.; Ingram, P.; Linton, R. W.; Gutknecht, W. F.; Mastin, P.; Shelburne, J. D., New techniques for imaging and analyzing lung tissue. *Environ Health Perspect* **1984**, *56*, 163-183.
7. Spengler, B.; Hubert, M., Scanning microprobe matrix-assisted laser desorption ionization (SMALDI) mass spectrometry: instrumentation for sub-micrometer resolved LDI and MALDI surface analysis. *J Am Soc Mass Spectrom* **2002**, *13* (6), 735-748.
8. Caprioli, R. M.; Farmer, T. B.; Gile, J., Molecular imaging of biological samples: localization of peptides and proteins using MALDI-TOF MS. *Anal Chem* **1997**, *69* (23), 4751-4760.
9. Luxembourg, S. L.; Mize, T. H.; McDonnell, L. A.; Heeren, R. M., High-spatial resolution mass spectrometric imaging of peptide and protein distributions on a surface. *Anal Chem* **2004**, *76* (18), 5339-5344.
10. Altelaar, A. F.; Luxembourg, S. L.; McDonnell, L. A.; Piersma, S. R.; Heeren, R. M., Imaging mass spectrometry at cellular length scales. *Nat Protoc* **2007**, *2* (5), 1185-1196.
11. Luxembourg, S. L.; Vaezaddeh, A. R.; Amstalden, E. R.; Zimmermann-Ivol, C. G.; Hochstrasser, D. F.; Heeren, R. M., The molecular scanner in microscope mode. *Rapid Commun Mass Spectrom* **2006**, *20* (22), 3435-3442.
12. Yoon, O. K.; Robbins, M. D.; Zuleta, I. A.; Barbula, G. K.; Zare, R. N., Continuous Time-of-Flight Ion Imaging: Application to Fragmentation. *Analytical Chemistry* **2008**, *80* (21), 8299-8307.
13. Llopart, X. B., R. Campbell, M. Tlustos, L. Wong, W. , Timepix, a 65k programmable pixel readout chip for arrival time, energy and/or photon counting measurements. *Nuclear Instruments and Methods in Physics Research, Section A* **2007**, *581* (1-2), 485-494.
14. Ballabriga, R.; Campbell, M.; Heijne, E. H. M.; Llopart, X.; Tlustos, L., The medipix3 prototype, a pixel readout chip working in single photon counting mode with improved spectrometric performance. *Ieee Transactions on Nuclear Science* **2007**, *54* (5), 1824-1829.
15. Vallerga, J.; McPhate, J.; Tremsin, A.; Siegmund, O., High-resolution UV, alpha and neutron imaging with the Timepix CMOS readout. *Nuclear Instruments & Methods*

1
2
3
4 *in Physics Research Section a-Accelerators Spectrometers Detectors and Associated*
5 *Equipment* **2008**, 591 (1), 151-154.

6
7 16. Anton, G.; Gebert, U.; Michel, T.; Rugheimer, T. K., A hybrid photodetector
8 using the Timepix semiconductor assembly for photoelectron detection. *Nuclear*
9 *Instruments & Methods in Physics Research Section a-Accelerators Spectrometers*
10 *Detectors and Associated Equipment* **2009**, 602 (1), 205-208.

11
12 17. Jungmann, J. H.; Macaleese, L.; Buijs, R.; Giskes, F.; de Snaijer, A.; Visser, J.;
13 Visschers, J.; Vrakking, M. J.; Heeren, R. M., Fast, High Resolution Mass Spectrometry
14 Imaging Using a Medipix Pixelated Detector. *J Am Soc Mass Spectrom* **2010**.

15
16 18. Bamberger, A.; Desch, K.; Renz, U.; Titov, M.; Vlasov, N.; Wienemann, P.;
17 Zwerger, A., Resolution studies on 5 GeV electron tracks observed with triple-GEM and
18 MediPix2/TimePix-readout. *Nuclear Instruments & Methods in Physics Research Section*
19 *a-Accelerators Spectrometers Detectors and Associated Equipment* **2007**, 581 (1-2), 274-
20 278.

21
22 19. Lange, M.; Pfaff, O.; Muller, U.; Brenn, R., Projectile fragment-ion fragment-ion
23 coincidences (PFIFICO) following fast ion impact on SF6. *Chemical Physics* **1998**, 230
24 (1), 117-141.

25
26 20. Baluya, D. L.; Garrett, T. J.; Yost, R. A., Automated MALDI matrix deposition
27 method with inkjet printing for imaging mass spectrometry. *Anal Chem* **2007**, 79 (17),
28 6862-6867.

29
30 21. Mikulec, B.; Clark, A. G.; Ferrere, D.; La Marra, D.; McPhate, J. B.; Siegmund,
31 O. H. W.; Tremsin, A. S.; Vallerga, J. V.; Clement, J.; Ponchut, C.; Rigal, J. M., A
32 noiseless kilohertz frame rate imaging detector based on microchannel plates read out
33 with the Medipix2 CMOS pixel chip. *Nuclear Instruments & Methods in Physics*
34 *Research Section a-Accelerators Spectrometers Detectors and Associated Equipment*
35 **2006**, 567 (1), 110-113.

36
37 22. Platkevic, M.; Bocarov, V.; Jakubek, J.; Pospisil, S.; Tichy, V.; Vykydal, Z.,
38 Signal processor controlled USB2.0 interface for Medipix2 detector. *Nuclear Instruments*
39 *& Methods in Physics Research Section a-Accelerators Spectrometers Detectors and*
40 *Associated Equipment* **2008**, 591 (1), 245-247.

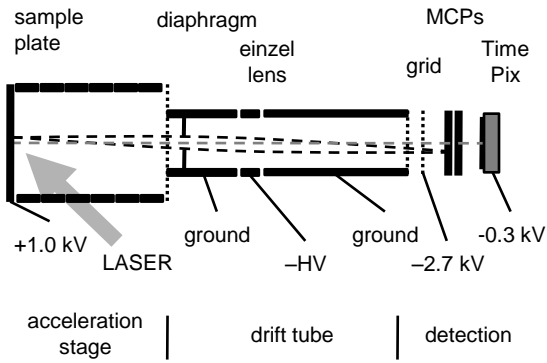
41
42 23. Harting, E.; Read, F. H.; Brunt, J. N. H., *Electrostatic lenses*. Elsevier Scientific
43 Pub. Co.: Amsterdam ; New York, 1976; p viii, 322 p.

44
45 24. McDonnell, L. A.; Heeren, R. M. A., Imaging mass spectrometry. *Mass*
46 *Spectrometry Reviews* **2007**, 26 (4), 606-643.

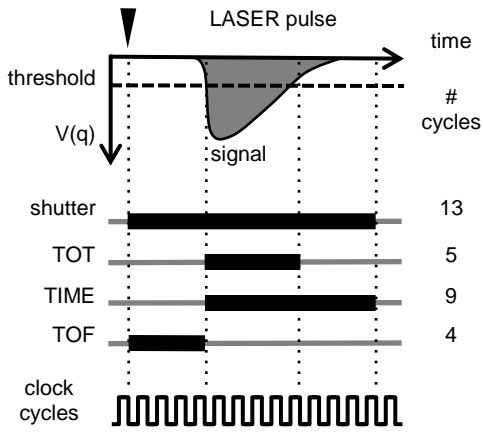
47
48 25. Caldwell, R. L.; Caprioli, R. M., Tissue profiling by mass spectrometry - A
49 review of methodology and applications. *Molecular & Cellular Proteomics* **2005**, 4 (4),
50 394-401.

51
52 26. Knochenmuss, R., A quantitative model of ultraviolet matrix-assisted laser
53 desorption/ionization. *Journal of Mass Spectrometry* **2002**, 37 (8), 867-877.

Figure 1



(a)



(b)

Figure 2

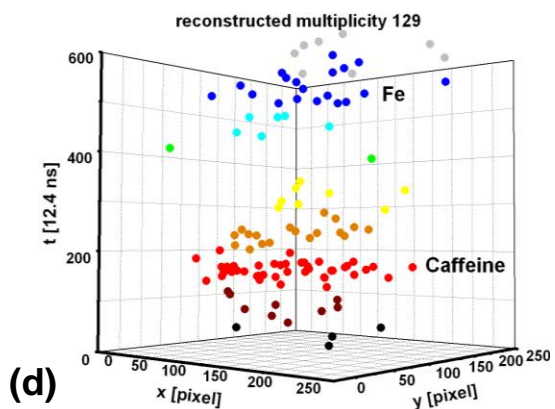
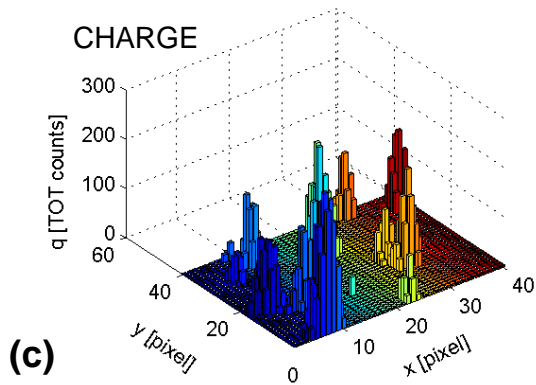
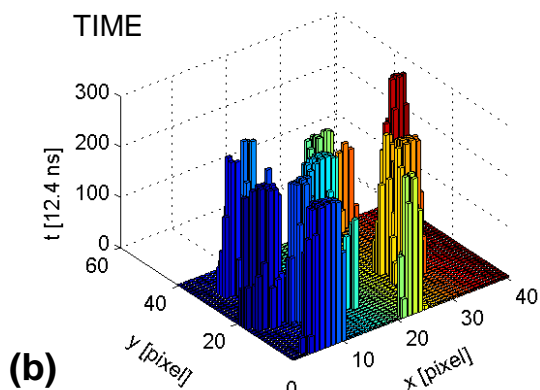
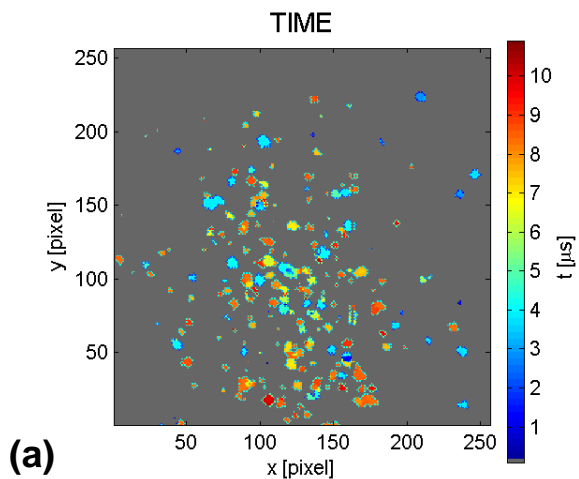


Figure 3

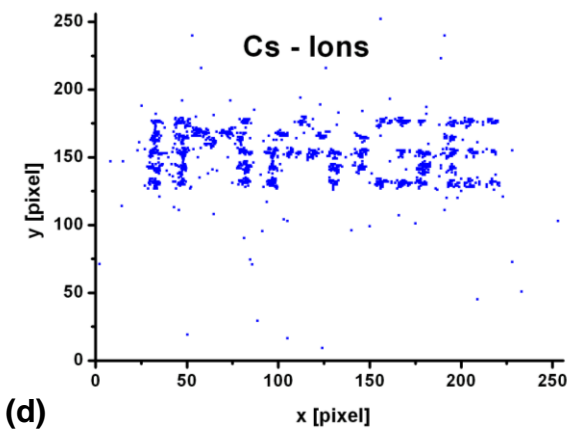
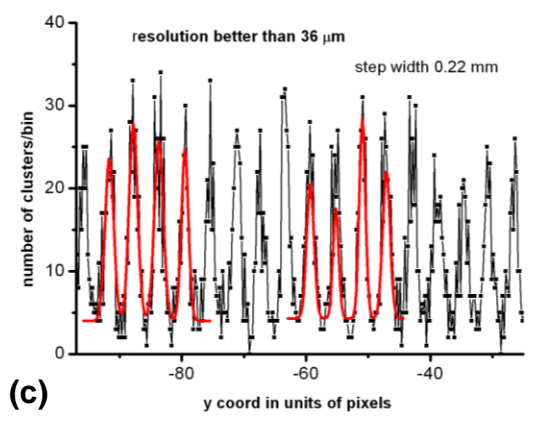
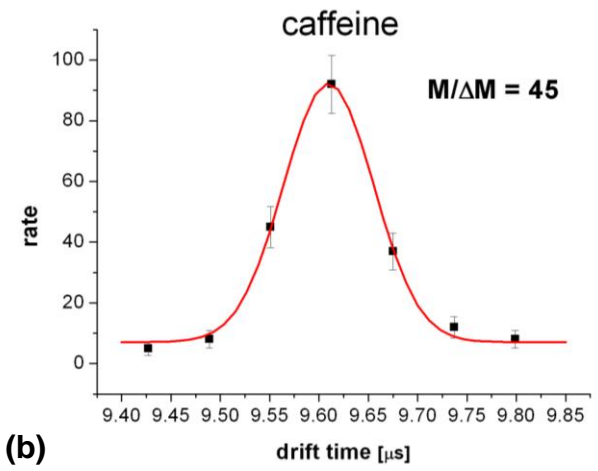
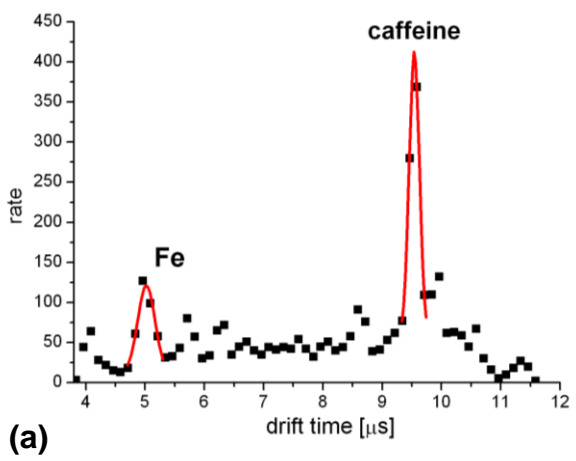
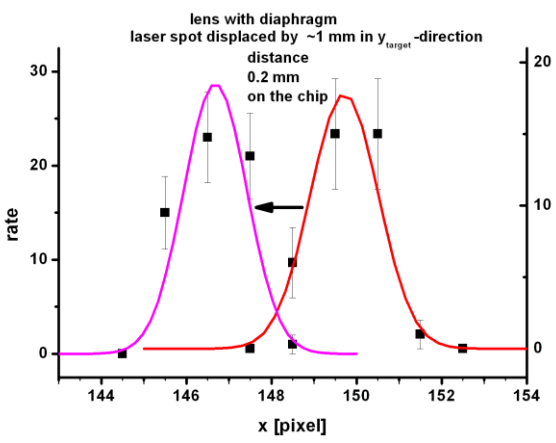
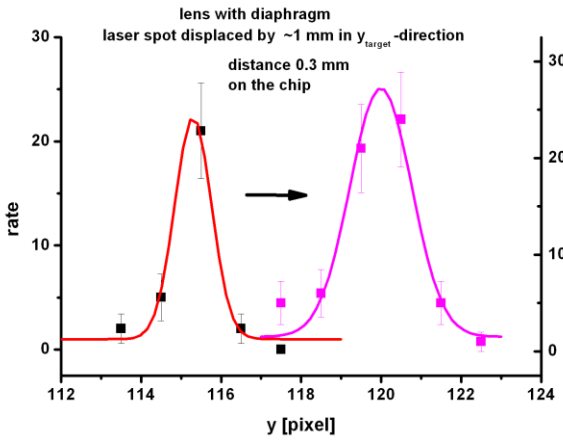


Figure 4

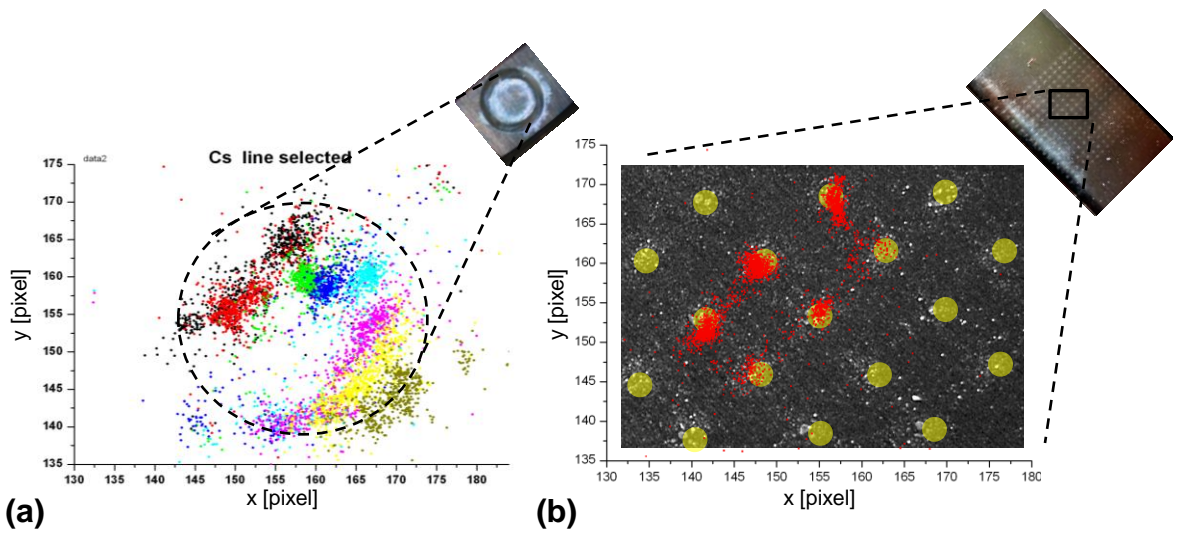


(a)



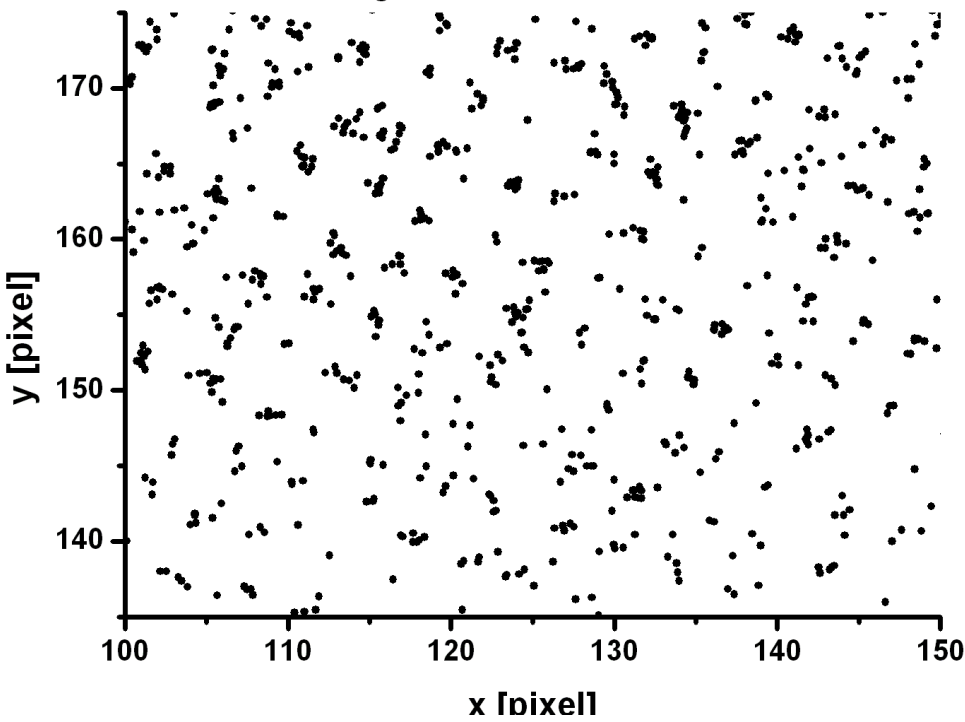
(b)

Figure 5

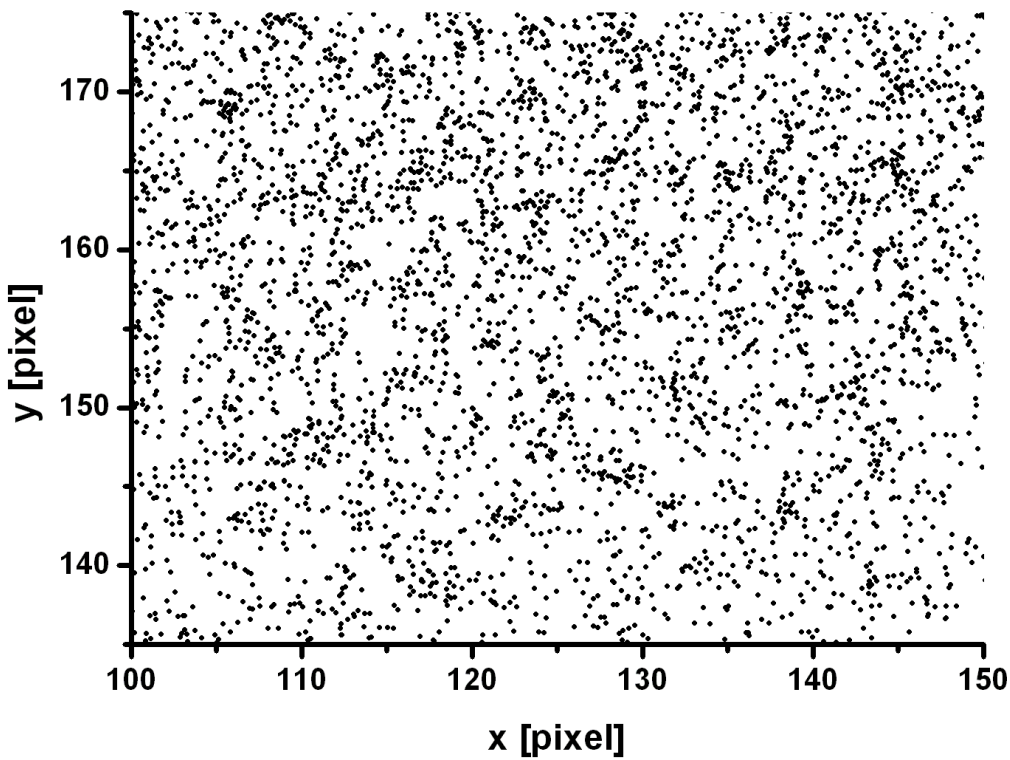


Supplemental Figure 1

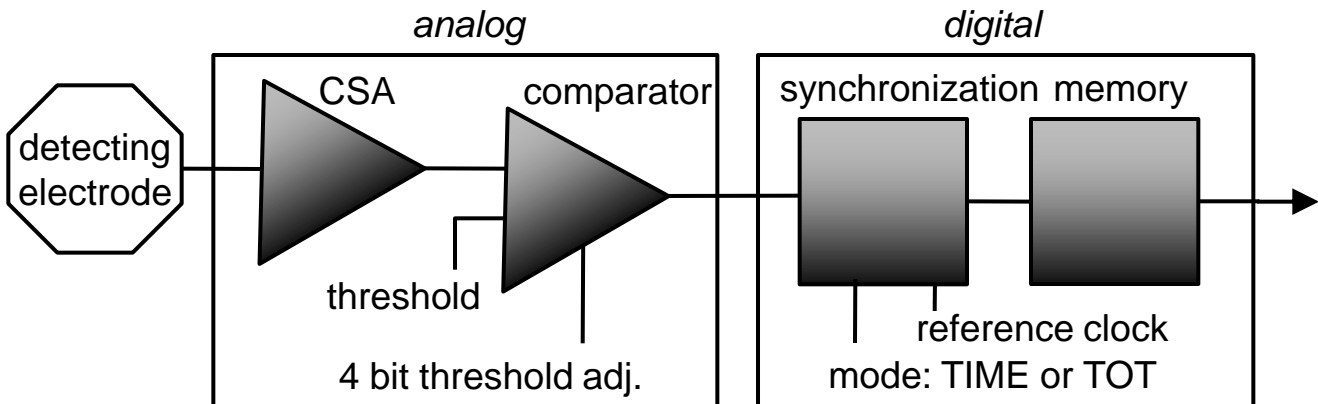
first grid at the end of the drift volume
field gradient 0 to 2.5 kV/cm



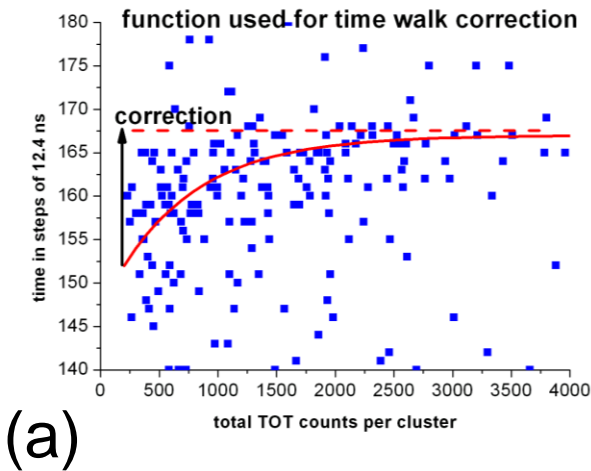
no structure without grid



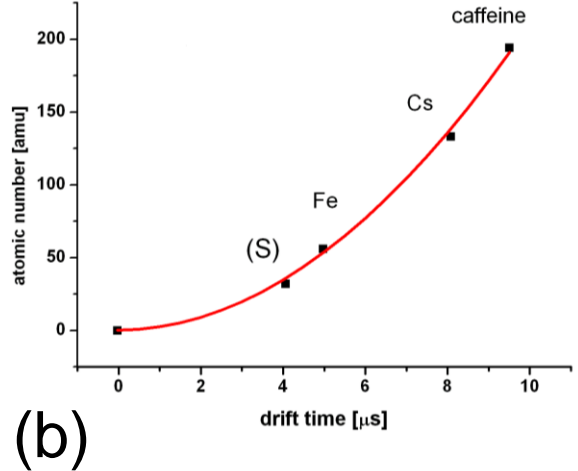
Supplemental Figure 2



Supplemental Figure 3

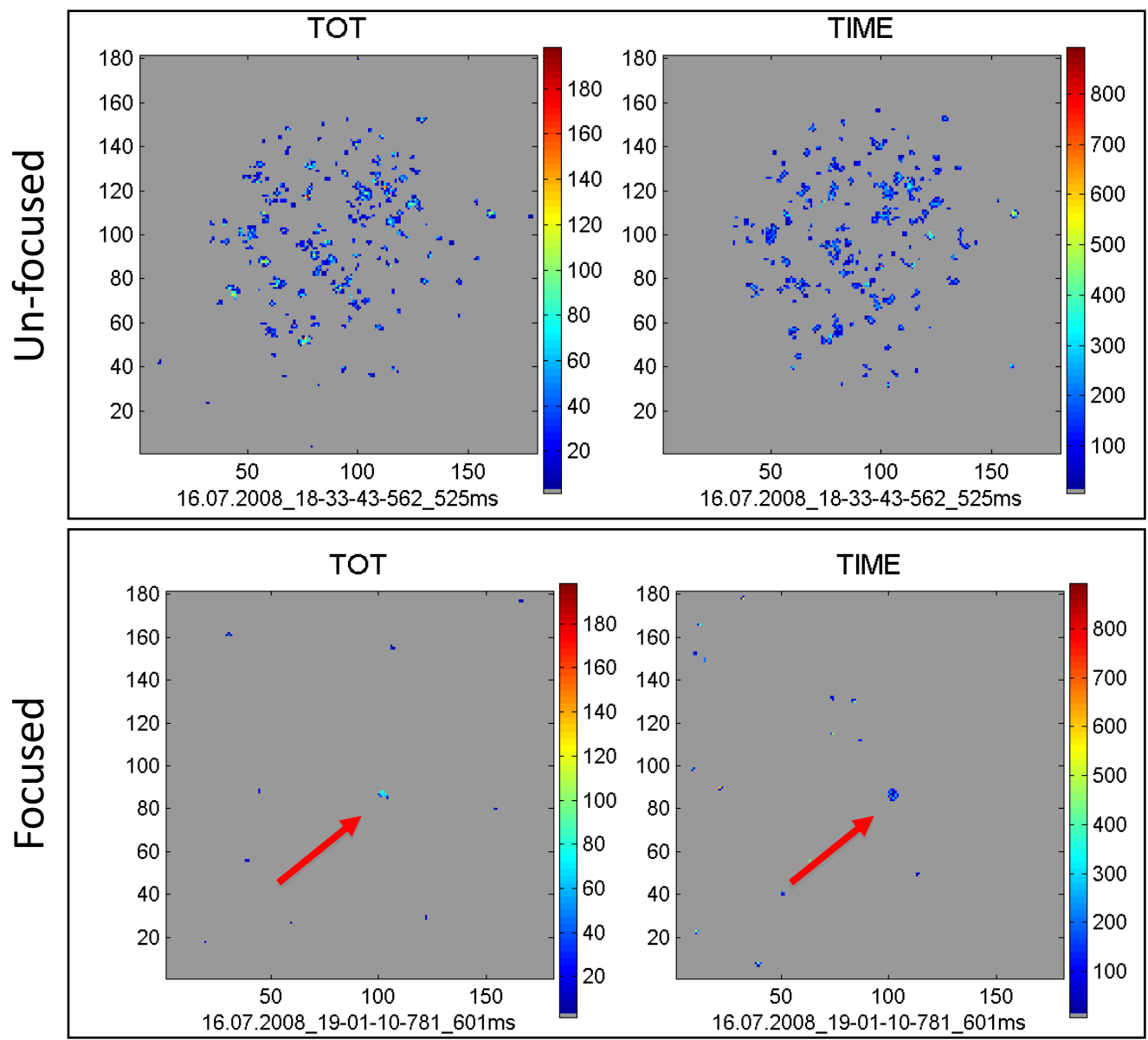


(a)

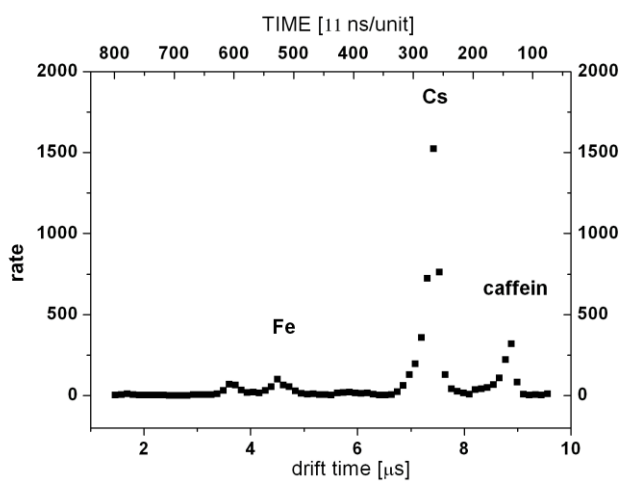


(b)

Supplemental Figure 4

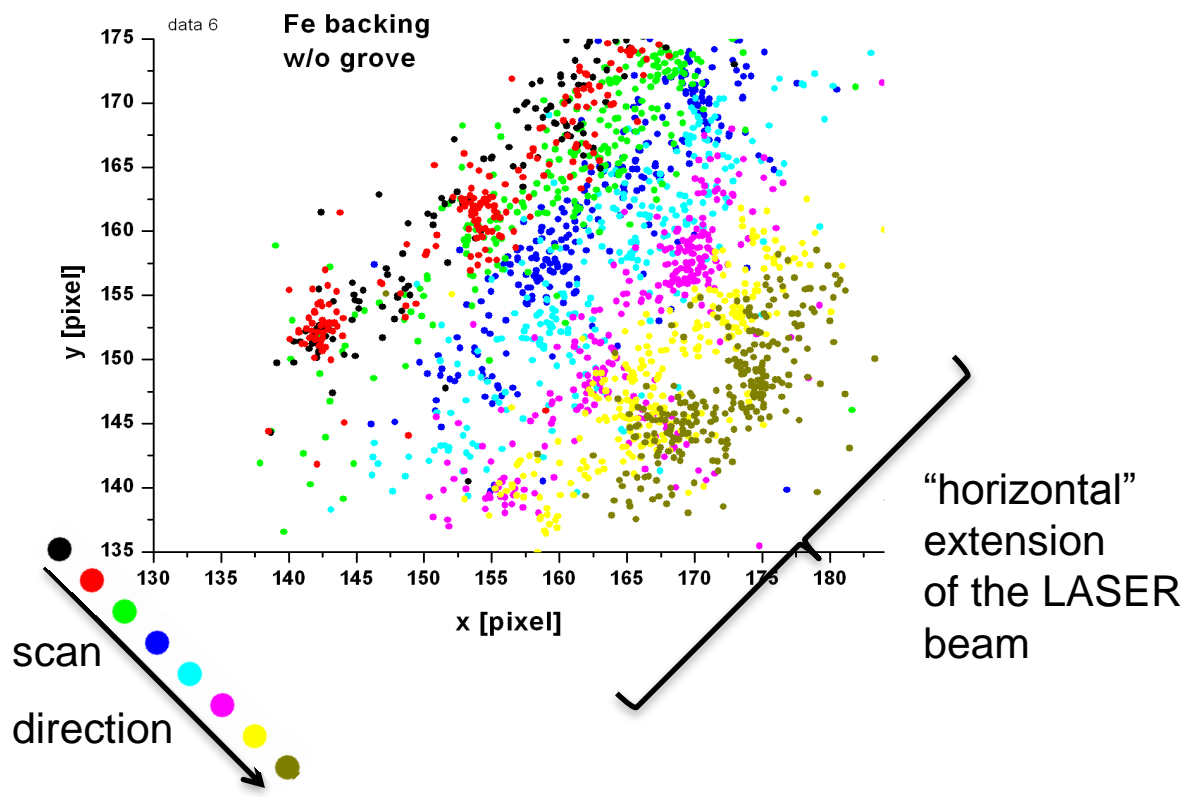


(a)

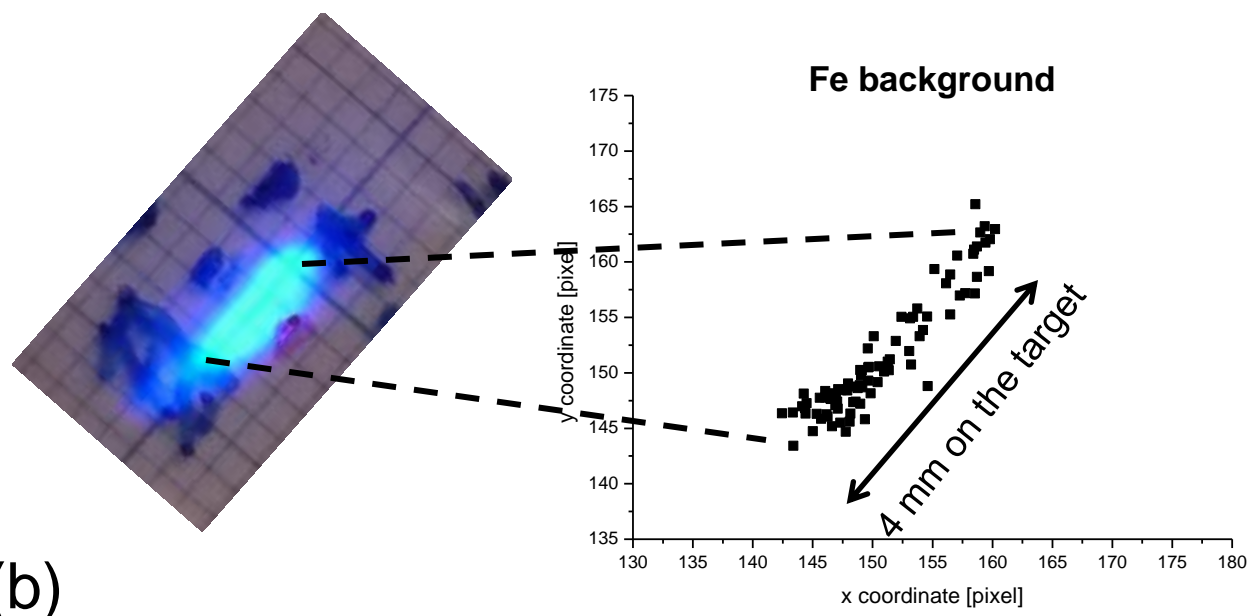


(b)

Supplemental Figure 5



(a)



(b)

Supplemental Information

[Click here to download Supplemental Information: DIMS-revision_supplemental_texts_022311.docx](#)